On Efficient External-Memory Triangle Listing

Yi Cui, Di Xiao, and Dmitri Loguinov, *Senior Member, IEEE*

Abstract—Discovering triangles in large graphs is a well-studied area; however, both external-memory performance of existing methods and our understanding of the complexity involved leave much room for improvement. To shed light on this problem, we first generalize the existing in-memory algorithms into a single framework of 18 triangle-search techniques. We then develop a novel external-memory approach, which we call *Pruned Companion Files* (*PCF*), that supports operation of all 18 algorithms, while significantly reducing I/O compared to the common methods in this area. After finding the best node-traversal order, we build an implementation around it using SIMD instructions for list intersection and PCF for I/O. This method runs 5-10 times faster than the available implementations and exhibits orders of magnitude less I/O. In one of our graphs, the program finds 1 trillion triangles in 237 seconds using a desktop CPU.

Index Terms—Triangle listing, external memory, graph algorithms

1 Introduction

Enormous size of modern datasets poses scalability challenges for a variety of algorithms and applications. One particular area affected by the explosion of big data is *graph mining* and, more specifically, motif discovery in large networks. Motifs are important building blocks of real-life networks in biology, physics, chemistry, sociology, and computer science [23], [25], [36], [37], [50], [53]. They capture *local* composition of graphs and allow reasoning about the underlying construction processes that result in the observed phenomena. Three-node cycles (i.e., triangles) have received the most attention, attracting research interest for over 35 years [29] and developing many applications in graph theory [8], [39], [51], [52], [54], bioinformatics [30], [37], computer graphics [20], databases [7], and social networks [9], [11], [17], [57].

Until recently [55], little was known about the CPU cost of triangle listing, its behavior under different acyclic orientations, and comparison across the different methods. Much of the previous work [3], [26], [33] utilized $O(.)$ bounds that were exactly the same for all involved methods (i.e., vertex/edge iterators). As it turns out [55], there are 18 algorithms for traversing the nodes of a triangle and handling the neighbors, which can be reduced to four equivalence classes from the CPU-cost perspective, each with its own optimal orientation. However, *external-memory* triangle listing remains largely unexplored. Given the same 18 options, how many different I/O classes are there, what node permutations do they require, and is it possible for some methods to simultaneously achieve optimal CPU and I/O complexity using the same orientation?

• *The authors are with the Department of Computer Science and Engineering, Texas A&M University, College Station, TX 77843. E-mail: {yi, di, dmitri}@cse.tamu.edu.*

Manuscript received 5 Sept. 2017; revised 5 June 2018; accepted 7 July 2018. Date of publication 23 July 2018; date of current version 3 July 2019. (Corresponding author: Dmitri Loguinov). Recommended for acceptance by K. Yi. For information on obtaining reprints of this article, please send e-mail to: reprints@ieee.org, and reference the Digital Object Identifier below. Digital Object Identifier no. 10.1109/TKDE.2018.2858820

1.1 State of the Art

Before delving into details, we discuss the I/O model used throughout the paper. A common assumption on I/O complexity in this field stems from [1], which prescribes that sequential reading of a file of size X requires cost X/B, where B is the block size. If this model somehow translates into I/O delay, it suggests that 100-MB blocks lead to $10\times$ faster operation than 10-MB blocks. In reality, however, both block sizes produce the same performance because read-ahead caching in disk firmware and RAID cards ensures that sequential data arrives into RAM at a constant speed S, regardless of block size B. Since the time to process the file is X/S, where S is a constant for a particular computer system, and all files involved in triangle listing in this paper are read sequentially, we assume the I/O complexity is measured in edges that must be retrieved from disk (or their byte equivalent). In case conversion between our notation and that of [1] is needed, all I/O formulas in the paper should be divided by B.

If m is the number of edges and $M \leq m$ is RAM size, previous implementations [4], [21], [26], [31] operate with a simple partitioning scheme that requires reading the graph $p = \lceil m/M \rceil$ times, for a total overhead of $pm \sim m^2/M$. In theory, better bounds in the form of $O(m^{1.5}/\sqrt{M})$ can be achieved [27], [41]; however, there are no reference implementations that use these methods. What makes previous work [4], [21], [26], [27], [31], [41] similar is that their performance does not depend on the traversal order within each triangle or preprocessing manipulations applied to the graph, which leaves little for additional investigation.

1.2 Main Results

Instead, we show below that there exists a technique for graph partitioning that maps the 18 triangle-listing algorithms into six distinct classes from the perspective of I/O cost. Their performance depends not only on the underlying graph, but also the acyclic orientation applied during preprocessing. We call this framework *Pruned Companion Files* (PCF) and demonstrate how all 18 methods can be combined under an umbrella of a single algorithm. Taking into account both I/O and CPU cost [55], we discover 16 unique

ways to perform triangle listing in external memory, none of which were known before.

Similar to the "small-degree assumption" of [21], [26], which are some of the fastest implementations in this area, our best method PCF-1B requires that RAM size be larger than the maximum out-degree d_i^+ under the descending-degree orientation θ_D. In this case, it is fairly simple to show that $\max_i d_i^+ \leq \sqrt{2m}$, which means that $M \geq \max_i d_i^+$ is a weak constraint for most practical problems. For example, 8 GB of RAM requires complete graphs with *no fewer* than 2×10^{18} edges (i.e., 8 exabytes). It is highly unlikely that such graphs, even if they existed, would be amenable to triangle listing using modern computer technology (i.e., the CPU cost of intersection would be enormous). For the same 8 GB, complete graphs would require at least 10^{27} operations.

While accurate modeling of PCF I/O complexity is difficult, we are still able to identify the best partitioning scheme and deduce its optimal permutation. In random graphs with Pareto degree sequences and shape parameter $\alpha > 4/3$, we also prove that the amount of data read from disk is upper-bounded by $\min(\gamma, p)m$, where γ is some constant independent of n. This produces a linear I/O bound under $M = O(1)$; in contrast, both of the previous techniques [26], [41] require M to scale as $\Theta(m)$ to achieve the same performance. We also demonstrate that our partitioning scheme keeps the number of list intersections and table lookups unchanged compared to RAM-only methods, which means that its runtime on a given graph remains fixed for all M as long as I/O is not the bottleneck.

To test these developments in practice, we build an implementation that combines PCF with a novel application of SIMD to edge iterator. Our solution, which we call PaCiFier, is benchmarked on a variety of real-world graphs, including four new ones that have not been examined for triangles before. Our densest graph (IRL-IP) contains over 1T triangles, while the largest (ClueWeb) has over 102B edges. Results show that PaCiFier is 1-2 orders of magnitude faster than the single-threaded vertex iterator MGT [26] and $5-10$ times quicker than the multi-threaded edge iterator PDTL [21]. More importantly, it achieves 10-50 times lower I/O complexity when RAM size is small compared to m.

Using a six-core Intel i7-3930K, PaCiFier finds 1T triangles in IRL-IP in just 237 seconds. Furthermore, with a single 3-TB magnetic hard drive and 256 MB of RAM, it can process our 358-GB ClueWeb (880B triangles) in 4.2 hours. Neither MGT nor PDTL can complete in the last case, but estimates put their runtime at 3 weeks (i.e., two orders of magnitude slower).

2 Generalized Iterators (GI)

Recent work [55] created a taxonomy of 18 vertex and edge iterators. They use figures to highlight the intuitive differences among the methods; however, the lacking formal treatment makes it difficult to extend these results to external-memory scenarios. We therefore introduce a new description framework, which we call *Generalized Iterators* (GI), that explicitly encodes the traversal order in each triangle. This allows us to parameterize a single algorithm to cover execution of all alternative methods.

2.1 Redundancy Elimination

Naive triangle-listing algorithms do not enforce order among the neighbors, which results in extremely inefficient operation. Besides discovering each triangle $3! = 6$ times, there are serious repercussions stemming from the fact that the number of pairs checked at each node is a quadratic function of its degree. Even on relatively small graphs, this can lead to $1000\times$ more overhead than necessary [55]. The redundancy can be eliminated by converting the graph into a directed version, in which quadratic complexity applies only to the *out-degree* (or *in-degree*, depending on the method), whose second moments[1] are kept significantly smaller than those of undirected degree. Assuming d_i is the undirected degree of node i and d_i^+ is its out-degree, sums in the form of $\sum_i d_i^2$ can be much larger than $\sum_i (d_i^+)^2$, both numerically and asymptotically.

Assume the nodes are first shuffled using some algorithm and sequentially assigned IDs from sequence $(1, 2, \ldots, n)$. This creates a total order across the nodes and is often called *relabeling*. A directed graph is then created, where out-neighbors of each node have smaller labels and in-neighbors have larger. This step is called *acyclic orientation*. Finally, in the directed graph, triangles Δ_{xyz} are listed in ascending order of the new labels, i.e., $x < y < z$. This procedure generalizes all previous efforts in the field, some of which perform only relabeling [33], [45], [47] and others only orientation [4], [21], [26], [31], [45], [48], [49]. The drawbacks of not doing both are discussed in [55].

2.2 Relabeling

Consider a simple (i.e., no self-loops) undirected graph $G = (V, E)$ with n nodes and m edges. Define θ to be a permutation of node IDs that starts with the ascending-degree order and re-writes the label of each node in position i to $\theta(i)$. Among the $n!$ possibilities, there are several named permutations [55], which include *ascending-degree* $\theta_A(i) = i$, *descending-degree* $\theta_D(i) = n + 1 - i$, *round-robin*

$$\theta_{RR}(i) = \begin{cases} \lceil \frac{n+i}{2} \rceil & i \text{ is odd} \\ \lfloor \frac{n-i}{2} \rfloor + 1 & i \text{ is even,} \end{cases} \quad (1)$$

and *complementary round-robin* $\theta_{CRR}(i) = \theta_{RR}(n + 1 - i)$, each of which optimizes a different class of triangle-listing methods [55]. The difference in CPU cost between the best and worst permutations can be orders of magnitude. Even worse, this ratio may be unbounded as $n \to \infty$ [55]. For a given permutation θ, define its *reverse* to be $\theta'(i) = n + 1 - \theta(i)$. This is a useful concept that allows detection of equivalence classes later in the paper.

Suppose G_θ is the relabeled graph under permutation θ. Its construction typically requires sorting the degree sequence of G using θ, re-writing the source nodes of each list, inverting the graph using external memory, and re-writing the source nodes again. It is also common during this process to drop all nodes with degree one since they cannot be part of a triangle.

2.3 Orientation

Define N_i to be the adjacency list of node i in G_θ. Note that variable i refers to the relabeled graph, e.g., the node with the i-th largest degree under θ_D. Using this notation, $d_i = |N_i|$ is the undirected degree of i. In general, $i \notin N_i$ because the graph is simple. Suppose the neighbors within each N_i are sorted ascending by their ID and G_θ is kept as a sequence of pairs $\{(i, N_i)\}_{i=1}^n$. Our next goal is to define

1. For a random variable X, the second moment is defined as $E[X^2]$.

notation that allows splitting arbitrary sets into values smaller/larger than a given pivot. The most immediate use is construction of in/out lists in the directed graph, but we will encounter other applications shortly.

Suppose $\mathbb{N}$ is the set of natural numbers and consider two finite sets $S, T \subseteq \mathbb{N}$. Then, let

$$(T, S)^+ = \{j \in S | j \leq \max(T)\} \tag{2}$$

be a subset of S that is bounded from above by the largest value in T. When T consists of a single element i, we simply write $(i, S)^+$. Similarly, define

$$(T, S)^- = \{j \in S | j \geq \min(T)\} \tag{3}$$

to contain elements of S no smaller than the minimum in T. Then, the out-list of i in the oriented graph is given by $N_i^+ := (i, N_i)^+$, while the corresponding in-list by $N_i^- := (i, N_i)^-$.

When the $+/-$ operator is specified by a variable φ, i.e., $(T, S)^\varphi$, we say that *S is φ-oriented by T*. This notation can be extended to other graph concepts. For example, G_θ^φ consists of tuples $\{(i, N_i^\varphi)\}$, where i is the source node and N_i^φ is its neighbor list, and $d_i^\varphi := |N_i^\varphi|$ is the corresponding degree in the directed graph. Define $1 - \varphi$ to be the *inverse* of operator φ, i.e., a plus becomes a minus and vice versa. It is then not difficult to see that $G_{\theta'}^\varphi$ is identical to $G_\theta^{1-\varphi}$, i.e., reversing the permutation is equivalent to inverting the orientation.

2.4 Search Order

Our focus is on algorithms from the family of vertex/edge iterators, which operate by visiting the three nodes of a triangle in sequential order. All such methods can be described using the following framework. Given six different ways to permute the nodes of a triangle, we next show how φ allows us to model the various *trajectories* (i.e., orders of examination) during search that result in exactly one listing of each triangle. Suppose i is the first visited node by an algorithm, $j \in N_i$ is the second, and $k \in N_i$ is the last one. The larger/smaller relationship between these nodes is what differentiates the various traversal orders. All possible combinations are captured by Fig. 1a, where each dashed arrow represents a φ-relationship between the two neighboring nodes. If labeled with a plus, a dashed arrow indicates that the source node is *larger* than the destination. The roles are reversed when the label is a minus. Note that unlike our earlier notation Δ_{xyz}, where the order $x < y < z$ was fixed, the relationship between (ijk) is fluid, i.e., changed by parameter $\bar{\varphi} = (\varphi_1, \varphi_2, \varphi_3)$.

Once the $\bar{\varphi}$ vector is chosen, the dashed arrows become oriented and are replaced with solid lines that specify greater-than relationships among the nodes. One example is shown in Fig. 1b, where $k > i > j$. A simple rule to remember is that a $+$ keeps the direction of the dashed arrow, while a $-$ reverses it. Out of the $2^3 = 8$ possible $\bar{\varphi}$ vectors, two produce loops, such as the one in Fig. 1c. These are invalid because they lead to a contradiction, e.g., $k > i > j > k$, which makes the orientation *cyclic*. The remaining six combinations are studied next.

2.5 Algorithms

In Algorithm 1, we create the *generalized vertex iterator* (GVI) that can handle all valid $\bar{\varphi}$ vectors. The method starts by populating all directed edges from $G_\theta^{\varphi_3}$ into a hash table.

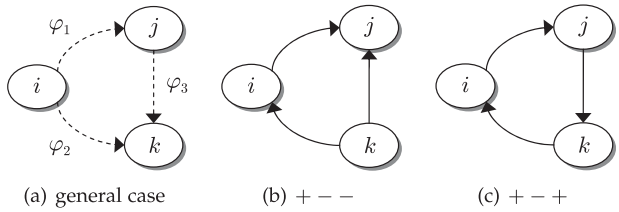

Fig. 1. Search-order operators in triangle listing.

The reason for using φ_3 is that the algorithm performs lookups of (j, k) against H, which we know from Fig. 1a have relationship φ_3. Then, for each node i, GVI creates two sets – the *hit list* X, from which j will be drawn, and the *local list* Y consisting of neighbors k that may complete a triangle. From Line 6, the algorithm examines every node $j \in X$, orients Y using φ_3 with respect to j, and checks the resulting pairs (j, k) against the hash table. Note that Line 7 is important for eliminating redundancy.

Algorithm 1. Generalized Vertex Iterator

```
1 Function GVI(φ̄)
2   build hash table H with all directed edges from G_θ^{φ3}
3   for i = 1 to n do
4     X = (i, N_i)^{φ1} ◁ neighbors of i in G_θ^{φ1} (hit list)
5     Y = (i, N_i)^{φ2} ◁ same in G_θ^{φ2} (local list)
6     foreach j ∈ X do
7       Y' = (j, Y)^{φ3} ◁ set Y φ3-oriented by j
8       foreach k ∈ Y' do
9         if (j, k) ∈ H then report triangle Δ_{sort(ijk)}
```

Algorithm 2. Generalized Lookup Edge Iterator

```
1  Function GLEI(φ̄)
2    for i = 1 to n do
3      X = (i, N_i)^{φ1} ◁ neighbors of i in G_θ^{φ1} (hit list)
4      Y = (i, N_i)^{φ2} ◁ same in G_θ^{φ2} (local list)
5      add elements of Y to hash table H
6      foreach j ∈ X do
7        Z = (j, N_j)^{φ3} ◁ neighbors of j in G_θ^{φ3} (remote list)
8        Z' = (i, Z)^{φ2} ◁ set Z φ2-oriented by i
9        foreach k ∈ Z' do
10         if k ∈ H then report triangle Δ_{sort(ijk)}
11     empty H
```

The next technique is the *generalized lookup edge iterator* (GLEI) whose operation is presented in Algorithm 2. The main difference begins in line 5, where GLEI populates the local list Y into a small hash table H. For each $j \in X$, the method constructs a *remote list* Z consisting of j's neighbors according to φ_3, orients it by φ_2 with respect to i, and checks its members against H. GLEI and GVI perform the same number of memory hits [55], with the only difference being the time needed to clear the hash table in Line 11.

The last method is the *generalized scanning edge iterator* (GSEI), which is described by Algorithm 3. It relies on sequential traversal of neighbor lists to perform set intersection in Line 9. This is in contrast to GLEI that uses hash tables for this purpose. The rest of the algorithm is quite similar. Before intersecting local and remote lists (Y, Z), the method orients them in Lines 7-8 to be consistent with Fig. 1a. Note that the former is done by GVI and the latter by GLEI. In practice, orientation of the local list Y imposes no additional overhead since j monotonically increases

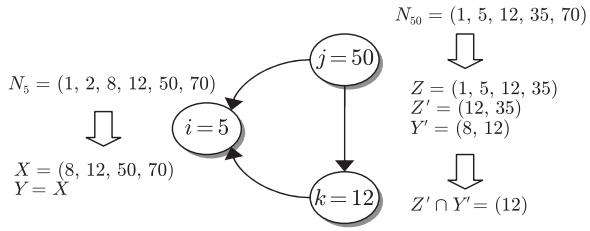

Fig. 2. Example of applying GSEI using $\bar{\varphi} = (--+)$.

within the loop, which is a consequence of $N_i^{\varphi_1}$ being sorted ascending. However, certain GSEI traversal orders require a binary search in the remote list Z to locate i [55].

Algorithm 3. Generalized Scanning Edge Iterator

```
1  Function GSEI(φ̄)
2    for i = 1 to n do
3      X = (i, N_i)^φ1 ◁ neighbors of i in G_θ^φ1 (hit list)
4      Y = (i, N_i)^φ2 ◁ same in G_θ^φ2 (local list)
5      foreach j ∈ X do
6        Z = (j, N_j)^φ3 ◁ neighbors of j in G_θ^φ3 (remote list)
7        Y' = (j, Y)^φ3 ◁ set Y φ3-oriented by j
8        Z' = (i, Z)^φ2 ◁ set Z φ2-oriented by i
9        K = Intersect (Y', Z')
10       foreach k ∈ K do report triangle Δ_sort(ijk)
```

Fig. 2 shows one example of GSEI operation, where $i = 5$ and $j = 50$. Since i is the smallest node in this triangle, we immediately get that $X = Y = (5, N_5)^- = (8, 12, 50, 70)$ are the neighbors of i with larger labels. After $j = 50$ is selected from X, the next step is to obtain j's out-neighbor list $Z = (50, N_{50})^+ = (1, 5, 12, 35)$. While $Z \cap Y$ correctly finds the triangle involving $k = 12$, this intersection performs unnecessary comparisons. We therefore can do better by shrinking Z to include only neighbors larger than i, which produces $Z' = (i, Z)^- = (12, 35)$. For similar reasons, Y can be reduced to contain only those neighbors smaller than j, which leads to $Y' = (j, Y)^+ = (8, 12)$. Performing intersection of Z' and Y' yields $k = 12$.

It should be noted that conversion from Z to Z' in the example of Fig. 2 requires a binary search; however, for the majority of methods this reduction comes at no cost (e.g., when $i \notin Z$). Furthermore, the figure shows existence of additional triangles involving nodes $(5, 50)$, i.e., $\Delta_{1,5,50}$ and $\Delta_{5,50,70}$. It is perfectly correct that they are ignored when $i = 5$ and $j = 50$ since the algorithm finds the former triangle using $i = 1$ and $j = 50$, while the latter is discovered when $i = 5$ and $j = 70$.

2.6 Taxonomy

A combination of Algorithms 1, 2, 3 comprises our *Generalized Iterators* (GI) framework. Analysis above shows that each of the main algorithms (i.e., GVI, GLEI, GSEI) admits six traversal orders and that this classification is exhaustive (i.e., no other patterns are possible). Table 1 assigns names to all methods based on their $\bar{\varphi}$, specifying whether the edge iterators require a binary search and how to relate (ijk) to $(xyz) = sort(ijk)$. For example T_2 first visits the middle node y, then the largest node z, and finishes with the smallest x. It is also not difficult to see that the method in Fig. 2 is E_6. In prior literature, T_1 can be found in [26], [31], [49], E_1 in [4], [21], [48], E_2 in [33], [45], E_3 in [13], [14], and E_5 in [47]. Methods T_1-T_3, E_1, E_3, E_4 are listed in [40].

TABLE 1
Taxonomy of Vertex/Edge Iterators

GVI	GLEI	GSEI	Binary Search	Vector $\bar{\varphi}$	i	j	k
T_1	L_1	E_1	No	$+++$	z	y	x
T_2	L_2	E_2	No	$-++$	y	z	x
T_3	L_3	E_3	No	$---$	x	y	z
T_4	L_4	E_4	No	$++-$	z	x	y
T_5	L_5	E_5	Yes	$+--$	y	x	z
T_6	L_6	E_6	Yes	$--+$	x	z	y

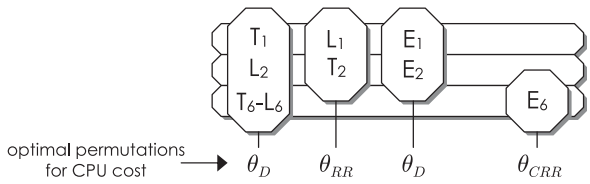

Fig. 3. Four CPU and three I/O classes.

While there are 18 techniques total, their CPU cost can be reduced to just four non-isomorphic classes [55]; however, this may no longer hold when I/O is taken into account. What can be said for sure is that reversing θ, or similarly inverting $\bar{\varphi}$, produces an identical method from the I/O standpoint. This allows reduction of scope to a subset of methods that cannot be converted into each other through inversion of $\bar{\varphi}$.

For example, keeping only methods that utilize G_θ^+ for remote edges, i.e., φ_3 is the plus operator, would eliminate rows $(3, 4, 5)$ in Table 1. In that case, Fig. 3 shows the position of the remaining 9 methods on a 2D plane, where the columns share the CPU cost, while the rows do the same for I/O. We use analysis from [55] to position the columns in order of increasing CPU complexity, with T_1 being the best and E_6 being the worst.The figure also provides the optimal permutation for CPU cost in random graphs using the results of [55]. While this is a good start, it is currently unknown if the rows do in fact differ in I/O cost, whether they can be split into multiple subrows depending on additional factors, and how their I/O relates to each other. This is our next topic.

3 Pruned Companion Files (PCF)

This section presents a general family of disk-based algorithms that supports all methods in Table 1. It also aims to achieve better I/O complexity than prior approaches.

3.1 Overview

It is important to discuss the performance objectives of external-memory algorithms before explaining our solution. There are four metrics that contribute towards the runtime of a method and its ability to handle large graphs. The first is the *triangle-identification time*. In GVI/GLEI, it is based on the number of lookups against H in Lines 9 and 10, respectively. In GSEI, it is determined by the amount of list intersections in Line 10. Examination of an item (i.e., edge or node) by these lines is an *elementary operation* for the corresponding algorithm. For a method $\mathcal{M}$ and orientation θ, suppose $c_n(\mathcal{M}, \theta)$ is the number of elementary operations, which we call the *CPU cost*, and $r(\mathcal{M})$ is the speed of these operations in items/sec. For a fixed pair (i, j), the CPU cost equals $|Y'|$ for GVI, $|Z'|$ for GLEI, and $|Y'| + |Z'|$ for GSEI. Then, the triangle-identification time is given by $c_n(\mathcal{M}, \theta)/r(\mathcal{M})$.

The second metric is the amount of I/O performed. Because all reads are sequential, this overhead is measured

by the length of adjacency lists across all graphs participating in the algorithm. The third metric is the *number of lookups based on hit list X* (i.e., Lines 6, 6, 5), which is generally a function of the partitioning scheme. This is in contrast to RAM-only operation, where this value is always fixed at m, i.e., the number of edges in G_θ. Finally, the last parameter is the *minimum amount of RAM supported by the method*.

It is possible that some of these metrics are tradeoffs of each other; however, if an ideal algorithm exists, it would simultaneously beat the other methods in all four categories.

3.2 Graph Partitioning

Because GSEI explicitly maintains remote and local lists, both GVI and GLEI can be viewed as its special cases that replace one of the lists with a hash table. For example, GVI uses H in place of scanning Z, while GLEI does the same for scanning of Y. As a result, any I/O partitioning scheme that handles GSEI can be adopted to work with the other two algorithms without incurring additional overhead. It should be noted that hash tables in Algorithms 1-2 refer to data structures already in RAM, i.e., there is no random access to disk. Specifically, GVI builds H from the current subgraph loaded entirely into memory. This subgraph is a chunk of $G_\theta^{\varphi_3}$ that is created by the algorithms below. GLEI creates H using the partitioned adjacency list $N_i^{\varphi_2}$ that is also present in RAM, as part of either the current subgraph or its companion file. Therefore, it is sufficient in the description of our I/O techniques to target only Algorithm 3.

In general, triangle-partitioning schemes work by placing one (or more) edges in some RAM buffer and then scanning the disk for discovery of the remaining edges that complete each triangle. Since node j and its neighbors k must be retrieved using random access, one crucial observation is that all methods require the *remote* edge (j,k) to be present in RAM, while the other two lists (X,Y) may be streamed from disk sequentially. This framework, coupled with general $\bar{\varphi}$ and the algorithms developed in this section, is what we call *Pruned Companion Files*.

Assume the set of nodes V is divided into p pair-wise non-overlapping and jointly exhaustive sets $\mathbf{V} = (V_1, \ldots, V_p)$. In a method we call PCF-A, we split $G_\theta^{\varphi_3}$ along the destination node of each pair $(j, N_j^{\varphi_3})$ to create a set of *remote-edge graphs*

$$G_\theta^r(l) = \{(j, N_j^{\varphi_3} \cap V_l)\}, \tag{4}$$

where $l = 1, 2, \ldots, p$. In a method we call PCF-B, we do the same along the source nodes

$$G_\theta^r(l) = \{(j, N_j^{\varphi_3}) | j \in V_l\}. \tag{5}$$

These technique are illustrated in Fig. 4 and their properties are given by the next result.

Theorem 1. *Algorithms 1, 2, 3 operating over PCF-A/B find each triangle exactly once. Furthermore, for a given graph G_θ, the triangle-identification cost $c_n(\mathcal{M}, \theta)$ remains constant for all p.*

Proof. First notice that every edge (j,k) belongs to a unique partition $G_\theta^r(l)$. Then, replacing $G_\theta^{\varphi_3}$ with $G_\theta^r(l)$ in Algorithms 1-3 and repeating for all $l = 1, 2, \ldots, p$, we immediately obtain that no triangle is missed or counted more than once.

To show that the triangle-counting overhead remains constant, we focus on GSEI, with the other methods being similar. Fix a node j and assume the length of its neighbor list Z after orientation by node i in Line 8 is given by q_{ij}. Note that list Y' is independent of the partitioning scheme and can be ignored. For RAM-only operation, the intersection cost related to j can be expressed as

$$\sum_{(i,j) \in G_\theta^{\varphi_1}} q_{ij}. \tag{6}$$

In PCF-A, assume the length of Z oriented by i in partition l is given by $q_{ij}(l)$. This leads to an overall cost for j

$$\sum_{l=1}^{p} \sum_{(i,j) \in G_\theta^{\varphi_1}} q_{ij}(l). \tag{7}$$

Since the partitions are mutually disjoint and exhaustive, it must be that for all i

$$\sum_{l=1}^{p} q_{ij}(l) = q_{ij}, \tag{8}$$

which yields the same cost in (7) as in (6) after changing the order of summations.

In PCF-B, the analysis is even simpler. Because j appears as the source node in exactly one partition, it experiences the same overhead (6) in that partition and zero in all others. □

This result shows that partitioning does not create any additional list-intersection cost, which allows us to focus on the remaining three objectives in the rest of the paper.

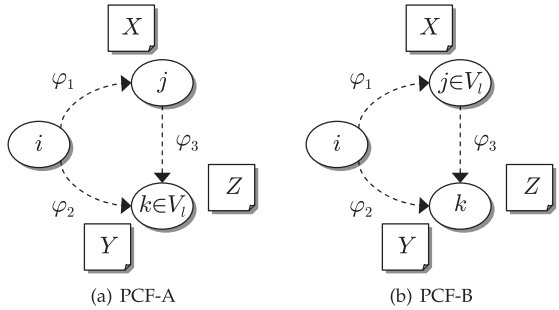

Fig. 4. Graph partitioning.

3.3 Partition Balancing

Assume M is the RAM size. To achieve the smallest p, each partition size $|G_\theta^r(l)|$ must equal M, which requires explicit balancing. Note that splitting the range $[1,n]$ into $p = \lceil m/M \rceil$ equal-size bins fails to accomplish this objective since permutation θ is degree-dependent. For example, with θ_D, smaller node IDs indicate larger degree. Therefore, nodes in the first bin may bring significantly more (or less depending on φ_3) edges into $G_\theta^r(l)$ than those in the last bin.

Balancing is accomplished by setting up boundaries $a_1, a_2, \ldots, a_{p+1}$ such that a node is included in V_l if and only if it belongs to $[a_l, a_{l+1})$. While $a_1 = 1$ and $a_{p+1} = n+1$ are obvious, the other values require more attention. For PCF-A in Fig. 4a, notice that inclusion of k into V_l implies that all edges from list $N_k^{1-\varphi_3}$ are placed into $G_\theta^r(l)$. Therefore, we must select the boundaries such that

$$\sum_{k=a_l}^{a_{l+1}-1} d_k^{1-\varphi_3} = M, \tag{9}$$

which can be accomplished in one pass over $G_\theta^{1-\varphi_3}$. For PCF-B in Fig. 4b, the roles of j, k are reversed, which leads to

$$\sum_{j=a_l}^{a_{l+1}-1} d_j^{\varphi_3} = M. \tag{10}$$

Balancing in PCF-A and B is equally fast, except the former requires existence of an inverted version of $G_\theta^{\varphi_3}$. If there is no sequence $\{a_k\}$ that satisfies (9) or (10), the corresponding method cannot run. We discuss the conditions for this to occur towards the end of the next section.

3.4 Companion Files

The fastest previous implementations [4], [21], [26], [31] use a framework that would scan the entire file $G_\theta^{\varphi_1}$ to obtain hit lists X and $G_\theta^{\varphi_2}$ for local lists Y. When $\varphi_1 = \varphi_2$, these files coincide, which cuts the overhead by half compared to other vectors $\bar{\varphi}$. Nevertheless, the amount of I/O produced by these schemes is still substantial, i.e., $pm \sim m^2/M$. Instead, our approach is to prune lists X, Y to be optimally suited for each partition l and write them into special *companion* files $G_\theta^c(l)$. Each of them, when paired with the corresponding remote-edge graph $G_\theta^c(l)$, allows identification of all triangles with either k (PCF-A) or j (PCF-B) in V_l.

Consider Algorithm 4, which is our one-pass solution to creating both companion and remote-edge files. If tuples $\{(i, N_i)\}$ are sorted by the source node i, Lines 3-5 simultaneously construct the three lists (X, Y, Z) by scanning multiple files in parallel; otherwise, only methods with $\varphi_1 = \varphi_2 = \varphi_3$ are supported. In Lines 7-14, the algorithm prepares the necessary lists for each partition l. Among these, Line 8 can be explained with the help of Fig. 4a. Notice that PCF-A can $(1 - \varphi_3)$-orient set X with respect to V_l without losing any relevant nodes j. Similarly Line 13 uses an observation from Fig. 4b that PCF-B can φ_3-orient Y with respect to V_l without omitting any essential nodes k.

Algorithm 4. One-Pass Graph Partitioning

```
1  Function PartitionGraph(method, φ̄, V)
2    for i = 1 to n do
3      X = (i, N_i)^{φ1} ◁ hit list from G_θ^{φ1}
4      Y = (i, N_i)^{φ2} ◁ local list from G_θ^{φ2}
5      Z = (i, N_i)^{φ3} ◁ remote list from G_θ^{φ3}
6      for l = 1 to p do ◁ go through each partition
7        if method = PCF-A then
8          X = (V_l, X)^{1−φ3} ◁ hit list oriented by V_l
9          Y = Y ∩ V_l ◁ keep only nodes in V_l
10         Z = Z ∩ V_l ◁ keep only nodes in V_l
11       else
12         X = X ∩ V_l ◁ keep only nodes in V_l
13         Y = (V_l, Y)^{φ3} ◁ local list oriented by V_l
14         Z = Z · 1_{i∈V_l} ◁ Z if i ∈ V_l and ∅ otherwise
15       Y' = Y ◁ local list to be written to G_θ^c(l)
16       if Z ≠ ∅ then
17         write record (i, Z) into G_θ^r(l)
18         if φ1 = φ3 then
19           X = X\Z ◁ further prune X
20         if φ2 = φ3 then
21           Y' = Y\Z ◁ further prune Y
22       if X ≠ ∅ and Y ≠ ∅ and |X ∪ Y| ≥ 2 then
23         write record (i, X, Y') to G_θ^c(l)
```

In Lines 18-19, where $\varphi_1 = \varphi_3$ indicates that sets X and Z may overlap, the algorithm drops redundant edges from X. The same operation applies to Y in Lines 20-21. Finally, the companion file receives triple (i, X, Y') if both hit list X and local list Y are non-empty, and there exist at least two nodes $j \in X$ and $k \in Y$ such that $j \neq k$.

Note that when $\varphi_1 = \varphi_2$, it is possible for X to overlap with Y. An important aspect of these cases is that Y is always φ_3-oriented against X. If additionally $Y' \neq \emptyset$, either $X \subseteq Y'$ or $Y' \subseteq X$ holds. Not only that, but the smaller list is always either at the bottom or top of the larger one. In such cases, only their union $X \cup Y'$ is written to disk, with an additional field indicating the offset that separates them. Algorithm 4 omits this detail to prevent clutter, but actual implementations should take it into account.

The main search function is shown in Algorithm 5. One noteworthy aspect is Line 8, which handles X being in RAM for PCF-A, and Line 10, which does the same for PCF-B. In the latter case, only nodes $j \in V_l$ should be included in the hit list, which explains the need for additional pruning. Since X being in RAM implies that Y is too, Line 11 uses $N_i(l)$ as the local list. Processing of individual nodes is given by Algorithm 6, which is identical to the corresponding section of GSEI, except it finds Z via the hash table rather than from the full graph $G_\theta^{\varphi_3}$.

4 Analysis

This section examines the introduced methods in comparison to each other. Our objective is to select a technique and its permutation so as to simultaneously maximize performance across all four criteria, if possible.

Algorithm 5. Disk-Based GSEI

```
1  Function FindTriangles(φ̄)
2    for l = 1 to p do
3      load G_θ^r(l) = {(i, N_i(l))} in RAM
4      build hash table H to map each i to its neighbor list
       N_i(l)
5      if φ1 = φ3 then ◁ possible for parts of X to be in RAM
6        foreach (i, N_i(l)) in RAM do
7          if method = PCF-A then
8            X = N_i(l) ◁ unrestricted hit list
9          else
10           X = N_i(l) ∩ V_l ◁ restrict hit list to V_l
11         ProcessOneNode (φ̄, i, X, N_i(l))
12     while not EOF(G_θ^c(l)) do
13       read one record (i, X, Y) from companion G_θ^c(l)
14       if Y = ∅ then
15         Y = H.find(i) ◁ local list must be in RAM
16       ProcessOneNode (φ̄, i, X, Y)
17     empty H
```

Algorithm 6. Modified GSEI Intersection

```
1  Function ProcessOneNode(φ̄, i, X, Y)
2    foreach j ∈ X do
3      Z = H.find(j) ◁ remote list is always in RAM
4      Y' = (j, Y)^{φ3} ◁ set Y φ3-oriented by j
5      Z' = (i, Z)^{φ2} ◁ set Z φ2-oriented by i
6      K = Intersect (Y', Z')
7      foreach k ∈ K do report triangle Δ_{sort(ijk)}
```

4.1 Overview

From this point on, we parameterize PCF with a specific $\bar{\varphi}$ from Table 1 by adding the corresponding row index. As

TABLE 2
Summary of PCF Algorithms Using Remote Graph G_θ^+

PCF	$G_\theta^r(l)$	Condition	X	Y'
1A	$(y,z)\to x$	$x\in V_l$	$z\to y$	$\emptyset$
2A	$(y,z)\to x$	$x\in V_l$	$y\leftarrow z$	$\emptyset$
6A	$z\to y$	$y\in V_l$	$x\leftarrow z$	$x\leftarrow y$
1B	$y\to x$	$y\in V_l$	$z\to y$	$z\to x$
2B	$z\to x$	$z\in V_l$	$y\leftarrow z$	$y\to x$
6B	$z\to y$	$z\in V_l$	$x\leftarrow z$	$x\leftarrow y$

before, we consider only rows $1, 2, 6$. When the A/B designation is non-essential, we omit it. For example, PCF-2 refers to $\bar{\varphi}=(-++)$ under both A/B, while PCF-2A narrows it down to the A partitioning scheme.

This creates the six I/O mechanisms in Table 2, where $i\to j$ signifies the out-list neighbor relationship, i.e., $j\in N_i^+$, and $i\leftarrow j$ the opposite, i.e., $j\in N_i^-$. Note that PCF-1A and 2A place two edges in RAM and load the third one from disk. This explains why their local list Y is always omitted from companion files. The remaining four techniques do the opposite – one edge is contained in $G_\theta^r(l)$ and two in $G_\theta^c(l)$. In three of these cases, edge direction is kept the same between X and Y, which ensures that either $X\subseteq Y'$ or $Y'\subseteq X$, with only one of them actually written to disk. Method PCF-2B is the lone exception with its $X\cap Y'=\emptyset$.

Table 3 summarizes the pruning rules and specifies the contents of each companion list. Notice that PCF-1B uses stricter conditions for achieving $X,Y\neq 0$ than PCF-1A and its $X\cup Y'$ is the same or smaller, which indicates that it out-performs its counterpart. Assuming θ_D, further scrutiny of companion lists in Table 3 reveals that PCF-1A produces less I/O than any of the remaining four methods, with PCF-6A/6B being essentially identical to each other.

4.2 Modeling I/O

Additional insight can be gleaned from bounding the size of companion files. Assume u_{il} is the length of i's hit list X' in $G_\theta^c(l)$ and v_{il} is that of $Y'\backslash X'$. Then, the total amount of companion I/O (in edges) is $H^c=H_X^c+H_Y^c$, where

$$H_X^c=\sum_{i=1}^{n}\sum_{l=1}^{p}u_{il},\quad H_Y^c=\sum_{i=1}^{n}\sum_{l=1}^{p}v_{il}, \tag{11}$$

and that for remote-edge graphs is

$$H^r=\sum_{i=1}^{n}|G_\theta^r(l)|=m. \tag{12}$$

Since H^r is constant for all $\bar{\varphi}$, comparison across the various approaches in Table 2 needs to involve only H^c. Closed-form derivation of accurate models for (11) currently appears intractable. Even ballparking the scaling rate is quite elusive for certain extremely heavy-tailed degree distributions [55]. Instead, we offer bounds achievable in two worst-case scenarios and leave more precise modeling for future work.

Theorem 2. *The companion I/O (in edges) of PCF-k can be upper-bounded as $H^c\le\zeta_k$, where*

$$\zeta_1=\sum_{i=1}^{n}\min\Big(\frac{d_i^+-1}{2},p-1\Big)d_i^+, \tag{13}$$

TABLE 3
Composition of Companion Lists in PCF

PCF	X	Y	Y'
1A	$N_i^+\cap[a_{l+1},n]$	$N_i^+\cap V_l$	$\emptyset$
1B	$(N_i^+\cap V_l)\cdot\mathbf{1}_{i\ge a_{l+1}}$	$N_i^+\cap[1,a_{l+1})$	Y
2A	N_i^-	$N_i^+\cap V_l$	$\emptyset$
2B	$N_i^-\cap V_l$	N_i^+	$Y\cdot\mathbf{1}_{i\notin V_l}$
6A	$N_i^-\cap[a_l,n]$	$N_i^-\cap V_l$	Y
6B	$N_i^-\cap V_l$	$N_i^-\cap[1,a_{l+1})$	Y

$$\zeta_2=\sum_{i=1}^{n}\min(d_i^+,p)d_i^-, \tag{14}$$

$$\zeta_6=\sum_{i=1}^{n}\min\Big(\frac{d_i^-+1}{2},p\Big)d_i^-, \tag{15}$$

where d_i^+ is the out-degree of i and d_i^- is its in-degree.

Proof. We only consider PCF-A since PCF-B uses similar arguments and produces the same bounds. It is not difficult to see that PCF-1A writes $H^c=H_X^c$ edges to companion files since its pruned hit lists Y' are always empty. First, notice that a list cannot be split into more than p chunks. Due to removal of overlap $X\cap Z$, we can do even better—the last partition V_p produces a hit list X only for neighbors $j\ge a_{p+1}=n+1$. Since no label can exceed n, there are actually at most $p-1$ partitions where $u_{il}\neq 0$. Therefore, $\sum_{l=1}^{p}u_{il}\le(p-1)d_i^+$.

Our second observation is that an out-list cannot be split into more than d_i^+ files. Then, the worst case arises when each V_l consists of a single node, where partition l contains the largest d_i^+-l out-neighbors of i. Thus,

$$\sum_{l=1}^{p}u_{il}\le\sum_{l=1}^{d_i^+}u_{il}\le\sum_{l=1}^{d_i^+}(d_i^+-l)=\frac{d_i^+(d_i^+-1)}{2}, \tag{16}$$

which combined with the first case yields (13).

For PCF-2A, the first case is very similar, except it uses the in-degree d_i^- and fails to remove the overlap $X\cap Z$. The second case writes the full in-neighbor list exactly d_i^+ times, which yields the result in (14). Finally, PCF-6A operates similar to 1A, except it uses the in-degree and fails to prune the lists as efficiently. Due to these small differences, its bound (15) is not perfectly symmetrical to (13). □

Using [55], we obtain that the I/O bound of PCF-1 is minimized by the descending-degree permutation θ_D, that of PCF-2 by round-robin θ_{RR}, and that of PCF-6 by ascending-degree θ_A. Furthermore, under their respective optimal permutations, (14) is strictly worse than (13). The bound of PCF-6 under θ_A rivals that of PCF-1 under θ_D, although it is still slightly higher due to a less-efficient pruning of overlap between (X,Y) and Z. The worst permutations corresponding to (13)-(15) are θ_A, θ_{CRR}, and θ_D, respectively [55].

For the asymptotics, we consider random graphs from [55]. This framework includes classical Erased Configuration Models (ECM) [10], [38], importance sampling [12], iterative edge rewiring [22], and other graph-construction methods [2], [15] in which the probability of edge existence between a pair of nodes is proportional to the product of their undirected degrees, i.e., $p_{ij}\sim d_i d_j$. At a high level, this process can be

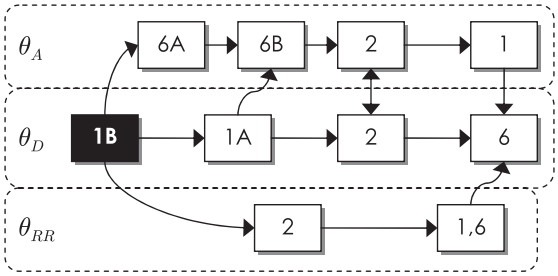

Fig. 5. Better-than relationships across the I/O of various PCF methods.

implemented by placing $2m$ node stubs into a shared pool, picking two stubs uniformly randomly at each time step, connecting them with an edge, and removing the selected stubs from the list. Duplicate edges and self-loops are either removed at the end or prevented from occurring in the first place, either way producing a simple graph.

Let $D_n \sim F_n(x)$ be the random degree of a node in a random graph of size n, where $F_n(x)$ is a distribution that changes with n to ensure the degree sequence is graphic and the conditions on p_{ij} are satisfied. Since we are interested in limiting cost as $n \to \infty$, distribution $F_n(x)$ is set to a truncated version of some fixed distribution $F(x)$, i.e., $F_n(x) = F(x)/F(t_n)$. Note that t_n is usually assumed to be $\Theta(\sqrt{n})$ to ensure that edge selection is sufficiently independent between different nodes and the constraints on p_{ij} hold. Truncation function t_n has no impact on the limit of CPU cost in [55] and is introduced for convenience of proofs. A common case of interest is the Pareto CDF $F(x) = 1 - (1 + x/\beta)^{-\alpha}$, which produces graphic sequences as $n \to \infty$ only when shape $\alpha > 1$ [5]. This implies that the expected degree in such graphs must be $O(1)$ and thus $m = \Theta(n)$ holds.

Observe that $F_n(x) \to F(x)$ as $n \to \infty$ and let $D \sim F(x)$ be a random variable drawn from the limiting distribution. Analysis in [55] shows how permutation θ affects the convergence point of sums in the form of $1/n \sum_i (d_i^+)^2$ and $1/n \sum_i d_i^+ d_i^-$. When these limits are finite, it is not difficult to see that the corresponding formulas in (13)-(15), which do not have normalization by n, are upper-bounded by linear functions of n. Specifically, under θ_D and $E[D^{4/3}] < \infty$, the scaling rate of (13) can be bounded as

$$\begin{aligned} \zeta_1 \; &< \; \sum_{i=1}^{n} d_i^+ \min(d_i^+, p) \le \min\Big(\sum_{i=1}^{n} (d_i^+)^2, p \sum_{i=1}^{n} d_i^+\Big) \\ &\le \min\Big(\sum_{i=1}^{n} (d_i^+)^2, pm\Big) \le \min(\gamma, p)m, \end{aligned} \tag{17}$$

where γ is some constant independent of n. For example, Pareto distributions $F(x)$ satisfy this requirement iff $\alpha > 4/3$. For PCF-2 and its best permutation θ_{RR}, the linear bound in (17) holds iff $\alpha > 1.5$ [55]. Note that (17) is strictly better than pm from prior implementations [4], [21], [26], [31]. When M is a constant, it is also better than theoretical results of [27], [41] whose $O(m^{1.5}/\sqrt{M})$ bound cannot be linear unless M grows at least as fast as m.

Based on Table 3, Theorem 2, and symmetry of PCF-1 A/6B and 1B/6A, Fig. 5 places the I/O of the various methods in relationship to each other under different permutations. When we do not differentiate between the PCF variants A/B of a given method, it is usually because they have similar I/O. From the picture, it emerges that PCF-1B with θ_D is globally the most efficient technique.

TABLE 4
Twitter I/O (in Billion Edges) under 16 MB of RAM

Permutation	1A	1B	2A	2B	6A	6B
θ_D	43.8	24.5	61.3	55.6	119.1	126.8
θ_{RR}	94.1	83.0	51.0	51.7	83.6	94.2
θ_A	125.7	118.4	54.8	61.7	25.5	44.2

4.3 I/O Comparison

For an illustration of the ideas presented earlier in this section, we employ the commonly considered Twitter graph [32] with 41M nodes and $m = 1.2$B edges. The file occupies 9.3 GB and its adjacency lists contain $2m = 2.4$B node IDs. We start with Table 4, which shows the size of companion files H^c. Observe that the predicted best-case permutations in each column (highlighted in gray) agree with earlier analysis. Additionally, notice that reversal of θ swaps PCF-A/B, switches PCF-1 to PCF-6, and maps PCF-2 back to itself. These effects were expected based on (13)-(15). Even though PCF-1 and PCF-6 are close under their optimal permutations, the former comes out ahead for the reasons discussed above.

We now examine how the methods scale as $M \to 0$. We dismiss PCF-6 due to its similarity to PCF-1. We also fix θ_D since it achieves the best CPU cost among the methods in Fig. 3. We vary RAM size from 1 GB down to 1 MB and plot the result in Fig. 6, where PCF-A cannot go lower than 16 MB due to inability to fit the largest in-degree into RAM. Observe that not only is PCF-1 more efficient than PCF-2, but the gap between the two grows as M decreases. As $M \to 0$ and $p \to \infty$, both methods converge towards their upper bounds, which are 150B in (13) and 360B in (14) [55]. The figure shows that PCF-1 is getting there at a slower pace than PCF-2.

We next analyze the scaling rate of our best method PCF-1B against the two previous models of I/O. Recall that the $pm \sim m^2/M$ technique was proposed by MGT [26], while the $O(m^{1.5}/\sqrt{M})$ bound is due to Pagh et al. [41]. Since there is no actual implementation for the latter, it is difficult to assess the constants inside $O(.)$. We thus take some liberty in assuming how this method would work in practice. It randomly colors the nodes using $c = \sqrt{m/M}$ unique values and splits the edges into c^2 files based on the color of source/destination nodes. It then combines three files of colors (ij, jk, ki) and runs MGT over the result. Since the size of each combined subgraph is $3m/c^2$, the I/O cost of the method is $9m^{1.5}/\sqrt{M}$ edges, which accounts for all c^3 combinations of triplets (ij, jk, ki).

The result for Twitter and $M \to 0$ is shown in Fig. 7a. After the initial jump, PCF-1B becomes parallel to Pagh's curve $1/\sqrt{M}$. Both of them scale significantly better than MGT's inverse linear function. In Fig. 7b we use random graphs with a Pareto degree distribution ($\alpha = 1.5$, $E[D] = 30$) to examine

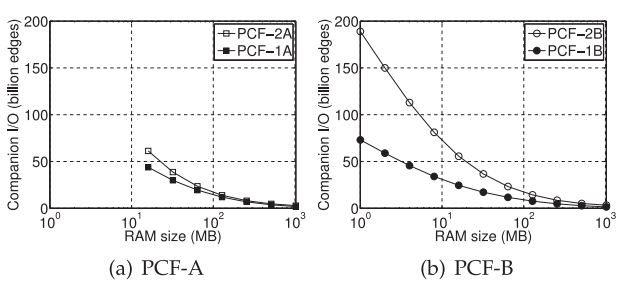

(a) PCF-A (b) PCF-B

Fig. 6. Scaling rate of PCF-1 on Twitter under θ_D.

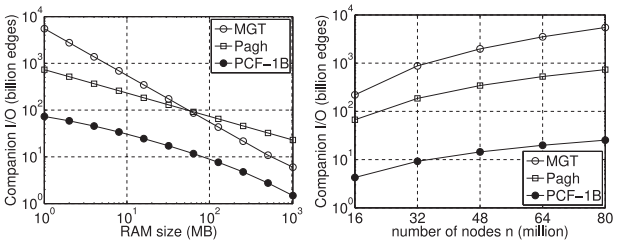

(a) Twitter (b) random graphs ($M = 1$ MB)

Fig. 7. Comparison against prior methods.

the scaling rate of I/O as $n \to \infty$. In this range, PCF-1B is roughly linear, while the other two methods grow significantly faster. As n increases, the ratio of MGT to PCF-1B jumps from 51 to 219, while that for Pagh from 15.5 to 29.3. To put this in perspective, $n = 80$M nodes requires 25B edges of I/O for PCF-1B, 734B for Pagh, and 5.5T for MGT.

A more in-depth asymptotic comparison is carried out in [18], which shows that PCF-1B is better than Pagh on sparse graphs, up to a factor of $\sqrt{n}$ (i.e., constant average degree and constant RAM size as $n \to \infty$). On the other hand, Pagh is better in dense graphs, also by up to a factor of $\sqrt{n}$ (i.e., complete graphs). This insight allows [18] to develop a new I/O method that beats both predecessors under all conditions and on all graphs.

4.4 CPU-I/O Tradeoffs

As it turns out, Fig. 3 splits into 16 different CPU-I/O complexity classes, i.e., two (A/B) for each of the 8 unique GI methods, with T_6-L_6 being a single entity. In the past, it was believed that GVI and GLEI were functionally identical. However, this is not the case when I/O is taken into account. For example, T_1 shares the I/O cost with L_1, but at lower CPU complexity. Similarly, it shares the CPU cost with L_2-L_6, while imposing less I/O. In the same vein, it was unknown until now whether E_1 and E_2 were interchangeable. Results above confirm that they are not.

These observations are emphasized using Table 5, where each I/O cell reports the best number achieved by either PCF-A or B. Observe that the best GVI is T_1, which exhibits optimal CPU and I/O complexity under θ_D. The decision is also easy for GSEI, where E_1 is the top contender. On the other hand, GLEI must choose which of the two objectives is more important – L_1 has the best I/O and L_2 the best CPU cost, both under θ_D. Other GLEI combinations are much worse.

4.5 Lookups and Minimum RAM

Recalling that PCF-B prunes X such that $X \subseteq V_l$ holds, while PCF-A does not, the next result follows immediately.

Theorem 3. *PCF-A issues H_X^c hit-list lookups and requires $M \geq \max_i d_i^{1-\varphi_3}$. PCF-B performs exactly m lookups and requires $M \geq \max_i d_i^{\varphi_3}$.*

In graphs with heavy-tailed degree and $M \ll m$, it is common that the hit list size $H_X^c \gg m$ (e.g., see Table 4). Therefore, for small RAM size, PCF-B should have a noticeably better CPU performance than PCF-A. In fact, its number of hash-table hits is optimal as it equals that in RAM-only algorithms.

In terms of restrictions on RAM, all considered methods PCF-1/2/6 have a plus for φ_3, which means that PCF-A lower-bounds M by the largest *in-degree*, while PCF-B by the largest *out-degree*. It is well-known that θ_D keeps the latter no larger than $\sqrt{2m}$; however, its maximum in-degree equals $\max_i d_i$, which can be significantly higher, i.e., up to $n-1$. Therefore, PCF-B under θ_D is definitively less restrictive than PCF-A. When the permutation is reversed, the bounds on in/out degree are swapped and PCF-A becomes better than PCF-B. Finally, θ_{RR} has both maximum in/out degree equal to $\max_i d_i$, which makes this permutation equally bad in both PCF-A/B.

TABLE 5
CPU-I/O Complexity Classes in Twitter under 16 MB of RAM

Under CPU-optimal permutation				Under I/O-optimal permutation			
Perm	GI	CPU	I/O	Perm	GI	CPU	I/O
θ_D	T_1	150B	24B	θ_D	T_1	150B	24B
	L_2	150B	56B		L_1	360B	24B
	T_6-L_6	150B	119B		E_1	511B	24B
	E_1	511B	24B	θ_{RR}	T_2	255B	51B
	E_2	511B	56B		L_2	63T	51B
θ_{RR}	L_1	255B	83B		E_2	63T	51B
	T_2	255B	51B	θ_A	T_6-L_6	123T	25B
θ_{CRR}	E_6	63T	45B		E_6	123T	25B

4.6 Summary

From the analysis above, two methods T_{1B} and E_{1B} emerge as clear winners within their respective classes (i.e., hash tables and scanning intersection). Among the 18 methods, they achieve the smallest companion I/O, perform the minimal number of hit-list lookups, impose the lowest RAM requirements, do not need to invert $G_\theta^{\varphi_3}$ during creation of $\{V_l\}$, and obtain (X, Y, Z) from a single file in Algorithm 4.

We next consider which of them has a smaller runtime. There are two aspects involved – the relative CPU cost

$$w_n := \frac{c_n(E_1, \theta_D)}{c_n(T_1, \theta_D)} \tag{18}$$

and the relative speed $s = r(E_1)/r(T_1)$. While [55] proves existence of random graphs where $w_n \to \infty$ as $n \to \infty$, ratio w_n is only $2-3$ in real graphs commonly studied in this area. Given that s is at least 20 on modern CPUs, it is conclusive that scanning edge iterators will remain the best option until graphs are discovered with much larger w_n.

5 Implementation

We now build a fast implementation of E_{1B} that takes advantage of SIMD for scanning the lists and PCF-B for I/O. We call this method PaCiFier and make it available in [19].

5.1 Intersection

Since E_{1B} spends almost all of its CPU time on intersection, it is crucial to address this bottleneck first. With support for SIMD in modern CPUs, we can exploit data-level parallelism and achieve a significant speedup compared to traditional CPU-based methods. We adopt the technique from [46], which utilizes STTNI intrinsics from SSE 4.2. They work on two 128-bit vector registers, treating them as four 32-bit or eight 16-bit integers. Fig. 8 shows how STTNI builds an all-to-all comparison matrix and outputs a vector of matches using just one instruction.

While 32-bit intersection is fast, better results can be procured by compressing labels into 16-bit numbers. This is

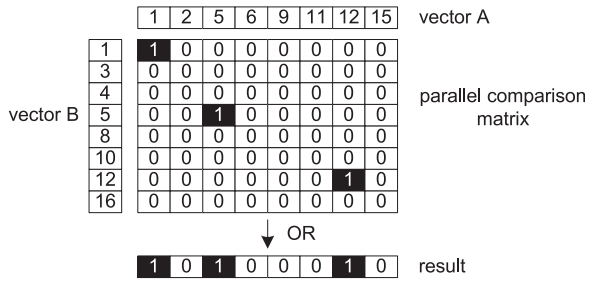

Fig. 8. Parallel intersection with STTNI.

performed by grouping node IDs into chunks that share the same upper 16 bits. For each chunk, PaCiFier additionally keeps its length and a list of the lower two bytes from each original label. This works well because all vertices are sequentially relabeled and adjacency lists are kept in ascending order. Besides almost doubling intersection speed, this method reduces graph size by approximately 50 percent.

For lists that are shorter than some threshold (e.g., 16), both compression and 16-bit intersection do not work well. In these cases, we keep the lists in 32-bit format and apply the branchless, scalar (i.e., non-SIMD) intersection from [28]. Note that employing STTNI, binary search [6], or SIMD galloping [35] over short lists produces worse results. A benchmark of some of these operations together with the Google Hash Table is shown in Table 6. With 1.8B operations/sec, PaCiFier's ratio s is a whopping 94.7. This places even more doubt that $\mathrm{T}_{1\mathrm{B}}$ will be competitive in the future, especially given that RAM bandwidth scales much faster than latency [44], i.e., s will continue increasing.

5.2 Relabeling and Orientation

Relabeling in degree-based permutations would normally require sorting pairs (degree, ID). This becomes a major bottleneck in preprocessing, especially for large graphs where these tuples do not fit in RAM. In contrast, we use an approach that decides the new labels without sorting the nodes. We first accumulate a histogram of degree frequency in one pass over pairs (i, d_i), which are kept separately from the adjacency lists $\{N_i\}$. Using a prefix sum of the histogram, we then establish the starting IDs for nodes of each unique degree value. Performing another scan of the tuples, we find the degree of each source node i in the histogram and create a mapping from old labels to the corresponding new IDs. This is shown in Fig. 9. Frequently accessed parts of the histogram typically fit in the L2 cache, which makes lookups against them extremely fast. If the mapping fits in RAM, PaCiFier performs a scan over the adjacency lists and rewrites all edges in one pass. Otherwise, it changes the source nodes, inverts the graph, and updates the source nodes again.

To reduce memory consumption, we use two simple rules to eliminate redundant nodes during orientation. First, PaCiFier drops all dangling vertices, i.e., those with degree $d_i = 1$, since they cannot participate in triangles. This technique is especially effective in power-law graphs, where a large fraction of nodes have degree 1. Second, source vertices with $d_i^+ = 0$ are discarded because intersecting against an empty list yields no useful results.

5.3 Parallelization

Scaling PaCiFier to multiple cores is rather straightforward. In Algorithm 5, the processing of each record $(i, X, Y) \in G_\theta^c(l)$ is an independent job, which allows multiple threads to work on different lists without interfering with each other. The lookup table H is read-only and can be safely shared by all worker threads without any locks. Assuming C available cores and hyper-threading, we run $2C$ worker threads and set the affinity mask to bind each thread to a dedicated core. This configuration ensures 100 percent CPU utilization for the entire execution and almost linear scalability with the number of cores (see below).

TABLE 6
Single-Core Speed (Intel i7-3930K @ 4.4 GHz)

Implementation	Speed (M/sec)
Hash table	19
Naive scalar intersection	264
Branchless intersection	416
SIMD 32-bit intersection	1,119
SIMD 16-bit intersection	1,801

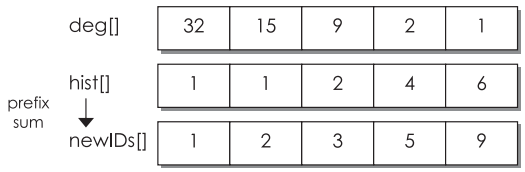

Fig. 9. Descending-degree relabel with a histogram.

5.4 Evaluation Setup and Datasets

Experiments use a six-core Intel i7-3930K @ 4.4 GHz, Asus Rampage IV Extreme motherboard, and quad-channel DDR3 RAM @ 2133 MHz. We compare PaCiFier against four methods with available implementations—RGP [14], DGP [14], MGT [26], and PDTL [21]. For the first three techniques, we use a single-threaded binary shared by the authors of [26]. For PDTL, we use a multi-threaded implementation that comes from the authors' github page.

We employ allthree standard graphs in the field—Live Journal (LJ) [26], US road maps (USRD) [26], Billion Triples Challenge (BTC) [24], WebUK [26], Twitter [32], and Yahoo [56]. Note that the original Yahoo graph has $n = 1.4$B, which reduces to 720M after removing zero-degree nodes. To cover a wider variety of options, we add two web crawls: IRLbot [34] and ClueWeb [16].[2] Out of the former, we extract domain, host, and IP-level graphs. Assuming $I(x)$ is the IP address of an authoritative nameserver for domain x, graph IRL-IP contains edges $I(x) \to I(y)$ iff $x \to y$ in IRL-domain, which may be useful for spam detection and ranking. The original ClueWeb dataset published online [16] does not contain any dynamic links and is limited to 7.9B edges [43]. We remedy this problem by running our HTML parser over all pages, which yields a much larger graph with 102B links.

Table 7 summarizes statistics of the graphs, where the old datasets require billion-scale intersection cost $c_n(E_1, \theta_D)$ and the new ones trillion-scale. The densest graph IRL-IP has an average degree 1,030, contains over 1T triangles, and requires 4.2T intersection operations. ClueWeb comes in at a hefty 358 GB, but neither its number of triangles nor CPU cost can top those of IRL-IP. Also note that the longest outlist in the table occupies just 35 KB of RAM, far smaller than the longest undirected neighbor set (i.e., 177 MB).

2. The new files can be downloaded from [19].

TABLE 7
Dataset Properties

Graph	Nodes (n)	Degree sum ($2m$)	Triangles	w_n	$c_n(E_1, \theta_D)$	Size	$E[d_i]$	$\max_i d_i$	$\max_i d_i^+$
LJ	4,846,609	85,702,474	285,730,264	3.01	2.1B	364 MB	17.7	20,333	685
USRD	23,947,347	57,708,624	438,804	2.37	25M	403 MB	2.4	9	4
BTC	164,660,997	772,822,094	28,498,939	1.59	3.5B	4.1 GB	4.7	1,637,619	646
WebUK	62,338,347	1,877,431,056	179,076,331,071	1.99	364B	7.5 GB	30.1	48,822	5,692
Twitter	41,652,230	2,405,026,390	34,824,916,864	3.38	511B	9.3 GB	57.7	2,997,487	4,102
Yahoo	720,242,173	12,869,122,070	85,782,928,684	1.47	433B	53.3 GB	17.9	7,637,656	1,540
IRL-domain	86,534,416	3,416,273,404	112,797,037,447	3.63	1.4T	13.3 GB	39.5	2,948,635	4,481
IRL-host	641,982,060	12,872,821,328	437,436,899,269	2.85	2.6T	52.7 GB	20.1	5,475,377	4,516
IRL-IP	1,588,925	1,636,848,800	1,032,158,059,864	3.17	4.2T	6.1 GB	1,030	669,776	8,915
ClueWeb	8,179,508,503	102,394,528,124	879,280,163,294	2.00	3.0T	358 GB	12.5	44,383,637	1,747

5.5 Preprocessing Time

RGP/DGP do not require preprocessing, while the other three methods manipulates the input graph G into a suitable format prior to actual listing of triangles. It is common to time the two phases separately, especially since the former can be performed once and the latter repeated many times on the same preprocessed data. Table 8 shows the result using a RAID system capable of reads at 1 GB/s. Even though PaCiFier is the only one performing both relabeling and orientation, it is still 2-8 times faster than MGT and up to 20 times faster than PDTL.

5.6 Triangle-Listing Time

We run the next set of tests using an 8-GB RAM constraint, which ensures that I/O is not a bottleneck for our RAID. As a result, Table 9 presents an evaluation of pure CPU efficiency of each algorithm. PaCiFier's performance is determined by the length of neighbor lists, i.e., efficiency of SIMD scanning. Compared to MGT, which implements T_1, its speedup varies from a factor of 13.6 on Yahoo to 78.6 on IRL-IP. In the latter graph, PaCiFier finds 1T triangles in 237 seconds, which translates into 17.7B neighbor checks/sec and 4.3B discovered triangles/sec using all six cores. Compared to PDTL, which is an optimized version of E_1 with MGT's partitioning scheme, PaCiFier achieves a 5-10× faster runtime.

The number of found triangles is consistent across the methods, except RGP/DGP fail to finish within 12 hours on several graphs, which we indicate with a dash. Additionally, MGT quits with an unrealistically small number of triangles (i.e., 170M) after spending 24K seconds on ClueWeb, which we show with an asterisk. Its traces point toward early termination before processing all of the partitions; however, unavailability of the source code prevents further analysis.

To put these results in perspective, Table 10 cites the runtime from prior work on Twitter and Yahoo. We split the algorithms into several categories—RAM-only, external-memory, and MapReduce. We report the number of utilized cores for the former two groups and cluster size for the last one. The first two methods in the table [47], [48] produce comparable numbers to those of PaCiFier, but using 3-6 times more late-model Xeon cores. Due to their RAM-only operation, we do not consider them competitors for PaCiFier. The next two techniques [4], [31] are extensions of RGP/DGP and MGT to multiple machines. They are generally faster than their respective predecessors, but still far slower than PaCiFier. The final four methods [17], [49], [42], [43] in the table are entirely disappointing – 87 to 572 times slower than PaCiFier while consuming substantially more resources.

5.7 Parallelization Efficiency

We now examine how PaCiFier scales with the number of cores, which indicates how well the algorithm benefits from additional CPU resources. As discussed earlier in section 5.3, PaCiFier's parallelization framework partitions the computation (i.e., triples (i, X, Y') from the companion file) into equal-sized jobs, which are processed lock-free by worker threads. As shown in Fig. 10, PaCiFier's runtime indeed scales almost linearly. The reason for a slightly suboptimal outcome is that certain auxiliary operations (e.g., indexing of $G^r_\theta(l)$ in Line 4 of Algorithm 5) are executed sequentially.

5.8 Effect of RAM: Bottlenecked by CPU

Next, we analyze the performance of each algorithm under varying RAM size. We showed earlier that PaCiFier's CPU cost was constant for all M. While the I/O complexity does increase as $M \to 0$, double buffering and prefetching can keep this overhead negligible until the disk becomes a bottleneck. Table 11 supports this discussion – using our RAID system, PaCiFier completes in virtually the same amount of time for all M in the range between 256 MB and 8 GB. The initial drop in runtime can be explained by smaller lookup tables and better cache locality; however, as M decreases further, SIMD becomes less efficient and this effect is reversed. While MGT is not bottlenecked by I/O either, PDTL increases its runtime by 49-116 percent at $M = 256$ MB. More interesting cases where the disk can no longer keep up with the computation are studied next.

5.9 Effect of RAM: Bottlenecked by I/O

For comparison of disk activity, we use the exact model $m\lceil m/M \rceil$ for MGT/PDTL and compute the size of all

TABLE 8
Preprocessing Time (Seconds)

Graph	MGT	PDTL	PaCiFier
LJ	2.2	1.0	1.7
USRD	2.0	1.4	2.0
BTC	18.8	11.6	8.9
WebUK	36.9	24.5	14.7
Twitter	88.9	38.4	24.5
Yahoo	295	276	149
IRL-domain	149	61.9	31.8
IRL-host	736	456	221
IRL-IP	33.9	19.1	8.5
ClueWeb	8,192	19,502	962

TABLE 9
Runtime (Seconds) With 8 GB of RAM

Graph	RGP	DGP	MGT	PDTL	PaCiFier
LJ	22.3	22.2	11.2	2.8	0.7
USRD	12.3	12.3	1.2	6.2	0.3
BTC	111	110	11.4	12.1	2.1
WebUK	1,299	891	599	93.6	17.1
Twitter	10,300	9,814	2,238	327	63.4
Yahoo	31,945	13,990	1,080	619	79.2
IRL-domain	17,717	16,919	5,946	849	148
IRL-host	–	–	11,099	1,773	367
IRL-IP	–	–	18,617	2,358	237
ClueWeb	–	–	*	13,782	1,737

TABLE 10
Results from Prior Work

Type	Algorithm	Runtime (sec)		Cores or servers
		Twitter	Yahoo	
RAM-only	[47]	101	–	16
	[48]	55.9	77.7	40
External	PATRIC [4]	552	–	200
	OPT [31]	469	819	6
MapReduce	[17]	36,300	–	47
	GP [49]	28,980	–	1,636
	TTP [42]	12,780	–	47
	CTTP [43]	5,520	61,920	40

companion files in PaCiFier by running Algorithm 4. Although DGP/RGP share the same $\Theta(m^2/M)$ asymptotic cost with MGT, these methods require two orders of magnitude more I/O due to slow convergence, which we omit from analysis. Instead, we contrast against MapReduce methods. The first one is GP [49], which uses at least $\rho = \lceil 3\sqrt{m/M} \rceil$ reducers and shuffles

$$\frac{30(\rho-1)(\rho-2)m}{\rho} \tag{19}$$

bytes of data [42]. A later method called TTP [42] reduces ρ by a factor of $\sqrt{3}$ and improves the shuffle to $20(\rho-1)m$.

Table 12 shows the I/O in bytes on the two largest graphs under consideration. PaCiFier starts off beating GP/TTP by a factor of 32-78 and MGT/PDTL by a factor of 3.7-9. This advantage keeps accumulating as M decreases. Eventually, PaCiFier develops a 58-195$\times$ lead over the former and $34-65\times$ over the latter as M reaches 256 MB. In the last scenario, the I/O phase of MGT/PDTL would require 34.5 hours to finish ClueWeb using our 1 GB/s RAID. With a magnetic hard drive (i.e., 100 MB/s read speed), this would take over two weeks. On the other hand, PaCiFier offers to lower these numbers to 32 minutes and 5.3 hours, respectively.

Armed with these predictions, we next investigate the actual runtime of MGT, PDTL, and PaCiFier in the setup of Table 12. To ensure that I/O is indeed a noticeable bottleneck for all RAM sizes, we equip our host with a single 3 TB hard drive (Hitachi Desktar 7K3000), capable of sequential reads at a maximum of 160 MB/s. The result, including both preprocessing delay and runtime, is shown for Yahoo

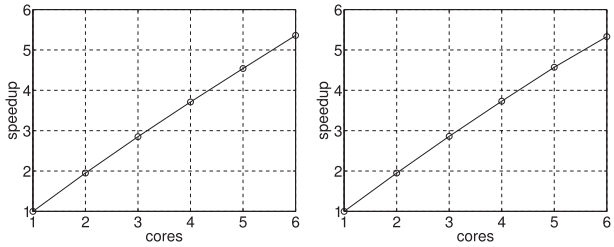

(a) Twitter (b) IRL-domain

Fig. 10. Speedup versus number of cores (8 GB of RAM).

TABLE 11
Runtime (Seconds)

Graph	RAM (MB)	MGT	PDTL	PaCiFier
Twitter	8,192	2,238	323	63.3
	4,096	2,248	327	63.2
	2,048	2,260	327	61.9
	1,024	2,285	347	61.0
	512	2,354	464	61.4
	256	2,487	1,003	67.2
IRL-domain	8,192	5,947	849	148
	4,096	5,976	851	144
	2,048	6,020	853	143
	1,024	6,090	898	143
	512	6,252	995	145
	256	6,540	1,484	149

TABLE 12
I/O Comparison

Graph	RAM (MB)	GP	TTP	MGT / PDTL	PaCiFier
Yahoo (in GB)	8,192	2,099	1,066	88.8	40.4
	4,096	3,271	1,599	177.6	47.6
	2,048	5,247	2,132	355.1	55.5
	1,024	7,632	3,198	710.2	64.8
	512	11,219	4,531	1,420	74.6
	256	16,408	6,663	2,841	84.4
ClueWeb(in TB)	8,192	47.4	19.2	3.91	0.69
	4,096	68.4	27.9	7.82	0.87
	2,048	99.8	40.2	15.6	1.10
	1,024	141.7	55.9	31.3	1.36
	512	204.6	80.4	62.6	1.64
	256	291.1	113.6	125	1.93

in Table 13. Since CPU operations (i.e., hash-table lookups) are no longer choking MGT, it manages to perform better than PDTL, both in orientation and triangle enumeration. However, PaCiFier is still much faster, by $5\times$ in the first row and $53\times$ in the last. More importantly, its scaling rate is much better, i.e., the PaCiFier runtime doubles within the span of the table, while that of MGT increases by a factor of 21. The MGT increase is sublinear (i.e., less than 32) because I/O is only partially a bottleneck in the first few rows.

Table 14 presents the result on ClueWeb. With 8 GB of RAM, MGT spends 52K seconds computing triangles, which we show in the table with an asterisk, but it is still unable to produce the correct result. We therefore omit running MGT on the remaining cases. PDTL takes longer than 4 days in all

TABLE 13
Runtime (Seconds) on Yahoo with Slow Hard Drive

RAM	MGT		PDTL		PaCiFier	
(MB)	pre	run	pre	run	pre	run
8,192	592	1,494	1,594	2,326	946	296
4,096	594	2,279	3,609	4,081	1,001	338
2,048	1,523	4,126	3,504	32,959	1,065	391
1,024	2,531	7,787			1,140	456
512	6,707	15,711	over 96 hours		1,224	524
256	7,066	31,696			1,310	591

TABLE 14
Runtime (Seconds) on ClueWeb with Slow Hard Drive

RAM	MGT		PDTL		PaCiFier	
(MB)	pre	run	pre	run	pre	run
8,192	18,650	*	23,853	53,946	10,190	5,318
4,096			24,310	109,915	11,301	6,261
2,048					12,952	7,711
1,024			over 96 hours		15,016	9,561
512					19,205	12,025
256					23,492	15,051

rows except the first two, where it is already 10-18× slower than PaCiFier. Focusing on the last row of the table, where the oriented and 2-byte compressed graph exceeds RAM by a factor of 664, PaCiFier completes 1.93 TB of I/O in 4.2 hours. This translates into 128 MB/s average disk-read speed. Since the peak rate of an empty 7K3000 HDD is 160 MB/s and magnetic drives become slower as they get full, the PaCiFier outcome appears very reasonable, especially considering PDTL's extrapolated time of 20.3 days (i.e., 116× slower).

6 Conclusion

We created a taxonomy of 18 triangle-listing methods using a unifying framework of Generalized Iterators (GI), developed a new set of algorithms (i.e., PCF) for external-memory operation of GI, and showed that it possessed better complexity than current implementations in the field. We then determined which of the 18 methods was the most efficient when both CPU and I/O objectives were taken into account and created a working solution that exhibited $5-10\times$ smaller runtime and orders of magnitude less I/O compared to the best previous techniques.

References

[1] A. Aggarwal and J. Vitter, "The input/output complexity of sorting and related problems," *Commun. ACM*, vol. 31, no. 9, pp. 1116–1127, Sep. 1988.

[2] W. Aiello, F. R. K. Chung, and L. Lu, "A random graph model for massive graphs," in *Proc. 32nd Annu. ACM Symp. Theory Comput.*, May 2000, pp. 171–180.

[3] N. Alon, R. Yuster, and U. Zwick, "Finding and counting given length cycles," *Algorithmica*, vol. 17, no. 3, pp. 209–223, Mar. 1997.

[4] S. Arifuzzaman, M. Khan, and M. Marathe, "PATRIC: A parallel algorithm for counting triangles in massive networks," in *Proc. 22nd ACM Int. Conf. Inf. Knowl. Manage.*, Oct. 2013, pp. 529–538.

[5] R. Arratia and T. M. Liggett, "How likely is an I.I.D. degree sequence to be graphical?" *Ann. Appl. Probability*, vol. 15, no. 1B, pp. 652–670, Feb. 2005.

[6] R. Baeza-Yates, "A fast set intersection algorithm for sorted sequences," in *Proc. Annu. Symp. Combinatorial Pattern Matching*, Jul. 2004, pp. 400–408.

[7] Z. Bar-Yossef, R. Kumar, and D. Sivakumar, "Reductions in streaming algorithms, with an application to counting triangles in graphs," in *Proc. Annu. ACM-SIAM Symp. Discrete Algorithms*, Jan. 2002, pp. 623–632.

[8] V. Batagelj and M. Zaveršnik, "Short cycle connectivity," *Elsevier Discrete Math.*, vol. 307, no. 3–5, pp. 310–318, Feb. 2007.

[9] L. Becchetti, P. Boldi, C. Castillo, and A. Gionis, "Efficient semi-streaming algorithms for local triangle counting in massive graphs," in *Proc. ACM SIGKDD Int. Conf. Knowl. Discovery Data Mining*, Aug. 2008, pp. 16–24.

[10] E. A. Bender and E. R. Canfield, "The asymptotic number of labeled graphs with given degree sequences," *J. Combinatorial Theory Ser. A*, vol. 24, pp. 296–307, May 1978.

[11] J. W. Berry, B. Hendrickson, R. A. LaViolette, and C. A. Phillips, "Tolerating the community detection resolution limit with edge weighting," *Phys. Rev. E*, vol. 83, no. 5, May 2011, Art. no. 056119.

[12] J. Blitzstein and P. Diaconis, "A sequential importance sampling algorithm for generating random graphs with prescribed degrees," *Internet Math.*, vol. 6, no. 4, pp. 489–522, 2011.

[13] N. Chiba and T. Nishizeki, "Arboricity and subgraph listing algorithms," *SIAM J. Comput.*, vol. 14, no. 1, pp. 210–223, Feb. 1985.

[14] S. Chu and J. Cheng, "Triangle listing in massive networks and its applications," in *Proc. 17th ACM SIGKDD Int. Conf. Knowl. Discovery Data Mining*, Aug. 2011, pp. 672–680.

[15] F. R. K. Chung and L. Lu, "Connected components in random graphs with given expected degree sequences," *Ann. Combinatorics*, vol. 6, no. 2, pp. 125–145, Nov. 2002.

[16] ClueWeb09 Dataset. [Online]. Available: http://www.lemurproject.org/clueweb09/

[17] J. Cohen, "Graph twiddling in a MapReduce world," *Comput. Sci. Eng.*, vol. 11, no. 4, pp. 29–41, Jul./Aug. 2009.

[18] Y. Cui, D. Xiao, D. B. Cline, and D. Loguinov, "Improving I/O complexity of triangle enumeration," in *Proc. IEEE Int. Conf. Data Mining*, Nov. 2017, pp. 61–70.

[19] Y. Cui, D. Xiao, and D. Loguinov, "IRL triangle datasets and code," Sep. 2016. [Online]. Available: http://irl.cs.tamu.edu/projects/motifs/

[20] I. Fudos and C. M. Hoffmann, "A graph-constructive approach to solving systems of geometric constraints," *ACM Trans. Graph.*, vol. 16, no. 2, pp. 179–216, Apr. 1997.

[21] I. Giechaskiel, G. Panagopoulos, and E. Yoneki, "PDTL: Parallel and distributed triangle listing for massive graphs," in *Proc. 44th IEEE Int. Conf. Parallel Process.*, Sep. 2015, pp. 370–379.

[22] C. Gkantsidis, M. Mihail, and E. Zegura, "The Markov chain simulation method for generating connected power law random graphs," in *Proc. SIAM Workshop Algorithm Eng. Experiments*, Jan. 2003.

[23] P. Gupta, V. Satuluri, A. Grewal, S. Gurumurthy, V. Zhabiuk, Q. Li, and J. Lin, "Real-time twitter recommendation: Online motif detection in large dynamic graphs," *Proc. VLDB Endowment*, vol. 7, no. 13, pp. 1379–1380, Aug. 2014.

[24] A. Harth, "Billion triples challenge data set," 2009. [Online]. Available: http://km.aifb.kit.edu/projects/btc-2009/

[25] T. Hocevar and J. Demsar, "A combinatorial approach to graphlet counting," *Bioinf.*, vol. 30, no. 4, pp. 559–565, Feb. 2014.

[26] X. Hu, Y. Tao, and C. Chung, "Massive graph triangulation," in *Proc. ACM SIGMOD Int. Conf. Manage. Data*, Jun. 2013, pp. 325–336.

[27] X. Hu, M. Qiao, and Y. Tao, "I/O-efficient join dependency testing, Loomis-Whitney Join, and triangle enumeration," *J. Comput. Syst. Sci.*, vol. 82, no. 8, pp. 1300–1315, Dec. 2016.

[28] H. Inoue, M. Ohara, and K. Taura, "Faster Set intersection with SIMD instructions by reducing branch mispredictions," *Proc. VLDB Endowment*, vol. 8, no. 3, pp. 293–304, Nov. 2014.

[29] A. Itai and M. Rodeh, "Finding a minimum circuit in a graph," *SIAM J. Comput.*, vol. 7, no. 4, pp. 413–423, 1978.

[30] Z. R. Kashani, H. Ahrabian, E. Elahi, A. Nowzari-Dalini, E. S. Ansari, S. Asadi, S. Mohammadi, F. Schreiber, and A. Masoudi-Nejad , "Kavosh: A new algorithm for finding network Motifs," *Bioinf.*, vol. 10, no. 318, Oct. 2009.

[31] J. Kim, W. Han, S. Lee, K. Park, and H. Yu, "OPT: A new framework for overlapped and parallel triangulation in large-scale graphs," in *Proc. ACM SIGMOD Int. Conf. Manage. Data*, Jun. 2014, pp. 637–648.

[32] H. Kwak, C. Lee, H. Park, and S. Moon, "Twitter graph," 2010. [Online]. Available: http://an.kaist.ac.kr/traces/WWW2010.html

[33] M. Latapy, "Main-memory triangle computations for very large (sparse (power-law)) graphs," *Elsevier Theor. Comput. Sci.*, vol. 407, no. 1–3, pp. 458–473, Nov. 2008.
[34] H.-T. Lee, D. Leonard, X. Wang, and D. Loguinov, "IRLbot: Scaling to 6 billion pages and beyond," *ACM Trans. Web*, vol. 3, no. 3, pp. 1–34, Jun. 2009.
[35] D. Lemire, L. Boytsov, and N. Kurz, "SIMD compression and the intersection of sorted integers," *Softw.: Practice Experience*, vol. 46, no. 6, pp. 723–749, Jun. 2016.
[36] L. A. A. Meira, V. R. Maximo, A. L. Fazenda, and A. F. D. Conceicao, "Acc-Motif: Accelerated network motif detection," *IEEE/ACM Trans. Comput. Biol. Bioinf.*, vol. 11, no. 5, pp. 853–862, Sep./Oct. 2014.
[37] R. Milo, S. Shen-Orr , S. Itzkovitz, N. Kashtan, D. Chklovskii, and U. Alon, "Network Motifs: Simple building blocks of complex networks," *Sci.*, vol. 298, no. 5594, pp. 824–827, Oct. 2002.
[38] M. Molloy and B. Reed, "A critical point for random graphs with a given degree sequence," *Random Structures Algorithms*, vol. 6, no. 2/3, pp. 161–180, Mar./May 1995.
[39] M. E. Newman, D. J. Watts, and S. H. Strogatz, "Random graph models of social networks," *Proc. Nat. Acad. Sci.*, United States America, vol. 99, no. Suppl. 1, pp. 2566–2572, Feb. 2002.
[40] M. Ortmann and U. Brandes, "Triangle listing algorithms: Back from the diversion," in *Proc. Meeting Algorithm Eng. Expermiments*, Jan. 2014, pp. 1–8.
[41] R. Pagh and F. Silvestri, "The input/output complexity of triangle enumeration," in *Proc. 33rd ACM SIGMOD-SIGACT-SIGART Symp. Principles Database Syst.*, Jun. 2014, pp. 224–233.
[42] H. Park and C. Chung, "An efficient MapReduce algorithm for counting triangles in a very large graph," in *Proc. 22nd ACM Int. Conf. Inf. Knowl. Manage.*, Oct. 2013, pp. 539–548.
[43] H. Park, F. Silvestri, U. Kang, and R. Pagh, "MapReduce triangle enumeration with guarantees," in *Proc. 23rd ACM Int. Conf. Inf. Knowl. Manage.*, Nov. 2014, pp. 1739–1748.
[44] D. A. Patterson, "Latency lags bandwidth," *Commun. ACM*, vol. 47, no. 10, pp. 71–75, Oct. 2004.
[45] T. Schank and D. Wagner, "Finding, counting and listing all triangles in large graphs, an experimental study," in *Proc. Int. Workshop Experimental Efficient Algorithms*, May 2005, pp. 606–609.
[46] B. Schlegel, T. Willhalm, and W. Lehner, "Fast sorted-set intersection using SIMD instructions," in *Proc. ADMS*, Sep. 2011.
[47] M. Sevenich, S. Hong, A. Welc, and H. Chafi, "Fast in-memory triangle listing for large real-world graphs," in *Proc. 8th Workshop Social Netw. Mining Anal.*, Aug. 2014, pp. 1–9.
[48] J. Shun and K. Tangwongsan, "Multicore triangle computations without tuning," in *Proc. 31st IEEE Int. Conf. Data Eng.*, Apr. 2015, pp. 149–160.
[49] S. Suri and S. Vassilvitskii, "Counting triangles and the curse of the last reducer," in *Proc. 20th Int. Conf. World Wide Web*, Mar. 2011, pp. 607–614.
[50] N. H. Tran, K. P. Choi, and L. Zhang, "Counting motifs in the human interactome," *Nature Commun.*, vol. 4, Aug. 2013, Art. no. 2241.
[51] N. Wang, J. Zhang, K.-L. Tan, and A. K. Tung, "On triangulation-based dense neighborhood graph discovery," *Proc. VLDB Endowment*, vol. 4, no. 2, pp. 58–68, Nov. 2010.
[52] D. J. Watts and S. Strogatz, "Collective dynamics of 'Small World' networks," *Nature*, vol. 393, pp. 440–442, Jun. 1998.
[53] S. Wernicke and F. Rasche, "FANMOD: A tool for fast network Motif detection," *Bioinf.*, vol. 22, no. 9, pp. 1152–1153, Feb. 2006.
[54] V. Willians and R. Williams, "Subcubic equivalences between path, matrix, and triangle problems," in *Proc. 51st IEEE Annu. Symp. Found. Comput. Sci.*, Oct. 2010, pp. 645–654.
[55] D. Xiao, Y. Cui, D. B. Cline, and D. Loguinov, "On asymptotic cost of triangle listing in random graphs," in *Proc. 36th ACM SIGMOD-SIGACT-SIGAI Symp. Principles Database Syst.*, Jun. 2017, pp. 261–272.
[56] Yahoo Altavista Graph, 2002. [Online]. Available: http://webscope.sandbox.yahoo.com/catalog.php?datatype=g
[57] Z. Yang, C. Wilson, X. Wang, T. Gao, B. Zhao, and Y. Dai, "Uncovering social network sybils in the wild," in *Proc. ACM SIGCOMM Conf. Internet Meas.*, Nov. 2011, pp. 259–268.

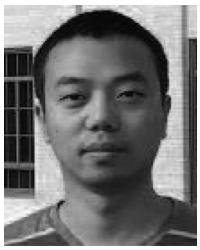

Yi Cui received the BS degree in computer science from Peking University, Peking, China, in 2010 and the PhD degree in computer science from Texas A&M University, College Station, Texas, in 2017. His research interests include graph mining, triangle enumeration, and web crawling.

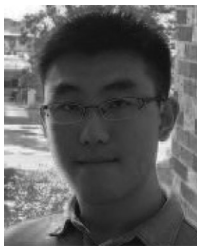

Di Xiao received the BS degree in software engineering from Beihang University, Beijing, China, in 2014. He is currently working toward the PhD degree in computer science at Texas A&M University, College Station, Texas. His research interests include graph algorithms, stochastic modeling, network sampling, and massive data computing.

Dmitri Loguinov (S'99–M'03–SM'08) received the BS degree with honors in computer science from Moscow State University, Russia, in 1995 and the PhD degree in computer science from the City University of New York, New York, in 2002. He is currently a professor with the Department of Computer Science and Engineering, Texas A&M University, College Station, Texas. His research interests include external-memory algorithms, P2P networks, information retrieval, congestion control, internet measurement, and modeling.